Materials Research. 2016; 19(1): 31-39
DOI:http://dx.doi.org/10.1590/1980-5373-MR-2015-0050

Synthesis by coprecipitation of india-stabilized zirconia and codoping with MoO_3, WO_3, $TaO_{2.5}$, or $NbO_{2.5}$ for application as thermal barrier coatings

***Roger Honorato Piva*[a]*, Diógenes Honorato Piva*[a], *Márcio Raymundo Morelli*[a]**

[a]*Laboratory of Ceramic Synthesis and Formulation, Materials Engineering Department / PPG-CEM, Federal University of São Carlos - UFSCAR, São Carlos, SP, Brazil*

Received: January 19, 2015; Revised: October 03, 2015; Accepted: November 17, 2015

Coprecipitation synthesis of nanocrystalline india-stabilized zirconia with high surface area and codoping with MoO_3, WO_3, $TaO_{2.5}$, or $NbO_{2.5}$ is reported. The concentration of codopants was defined by the charge-compensating mechanism. Ethanol washing followed by azeotropic distillation and freeze drying were compared as dehydration techniques for the gels. As determined by XRD and Raman scattering, 9 mol% of $InO_{1.5}$ plus charge-compensating dopants is sufficient to completely stabilize the high-temperature tetragonal phase of zirconia. The effect of alloying hexavalent and pentavalent oxides was secondary compared to the $InO_{1.5}$ concentration in the retention of the tetragonal structure. Improved specific surface area of 106.1 $m^2 g^{-1}$ and crystallite size between 8 and 9 nm were achieved through ethanol washing and subsequent azeotropic distillation even after calcination at 600 ºC. This result is attributed to the effect of the incorporation of ethoxy and butoxy groups after the treatment of the gels in organic medium, as detected by FT-IR spectroscopy and DSC/TG.

Keywords: *Zirconia; Thermal barrier coating; Coprecipitation; Azeotropic distillation; Freeze drying.*

1. Introduction

Thermal barrier coatings (TBC) have been widely used to protect metallic parts from high temperatures in gas turbines[1,2], providing substantial benefits to the engine[3]. TBC acts as an insulating surface, reducing the underlying metal temperature by as much as 150 °C[4,5], therefore enabling the operation of metal-based components without melting or high-temperature corrosion. Also, the application of TBC allows higher inlet temperatures of the gas turbine, thereby reducing the amount of cooling air and increasing the volume of the working gas. These are key factors to improve the efficiency of land-based turbines for electrical power generation[4].

Although some new systems are being studied[6,7], yttria-stabilized zirconia (YSZ) is still the main industrial TBC material[8]. However, increasing the turbine temperature using YSZ coatings is limited. One restriction arises from the phase stability of tetragonal zirconia at high temperatures. Considerable improvements in this case have been found by alloying $YNbO_4$ and $YTaO_4$ to zirconia[9,10]. Another drawback is the low corrosion resistance of YSZ against molten salts[2]. As the variety of fuels that can be used in gas turbines is quite extensive, there is a growing interest in non-traditional fuels such as petroleum coke or residual and heavy oils[4,11,12]. In turbines burning these low-quality fuels, a high concentration of impurities, namely vanadium, phosphorus, and sulfur form salts responsible for the shortening of the YSZ-coating lifetime[11,13]. At high temperatures, these molten salts are responsible for the depletion of stabilizing Y^{3+} ions from the YSZ lattice, resulting in coating cracks and detachment due to the 4-vol% expansion associated with the tetragonal-to-monoclinic phase transformation[1,3].

It is well known that the corrosion resistance of zirconia coatings can be improved by selecting and employing different stabilizers instead of yttria, since the nature of the stabilizer cation has been considered to be the most important factor affecting the corrosion resistance of zirconia-based TBCs[14,15]. Jones et al.[16,17], who attempted to identify the most corrosion-resistant stabilizer, reported that the resistance of In_2O_3 against molten salts is greater than that exhibited by Y_2O_3, suggesting that 7.8–12.2 mol% $InO_{1.5}$-stabilized zirconia (InSZ) may be an alternative coating to YSZ for gas turbines burning low-quality fuels. In the binary system ZrO_2–$InO_{1.5}$[18], stabilization of metastable tetragonal phase has been reported alloying up to 9 mol% de $InO_{1.5}$, whereas the cubic phase stabilization starts at higher $InO_{1.5}$ additions. Despite its efficacy against corrosion by molten salts, a major problem associated with InSZ is the volatilization of In_2O_3[19], which results in poor-quality and inhomogeneous coatings. To date, few attempts have been made to lower the volatilization of In_2O_3 in InSZ coatings. The most promising approach was reported by Hill et al.[20], that the pre-reaction of certain oxides, such as Sm_2O_3 and Gd_2O_3, with In_2O_3 prevents loss of indium due the formation of a stable and less volatile perovskite compound. It appears that the alloying of a ternary oxide into InSZ can be the main route to improve its thermal stability. Considering this approach, in this paper we apply the concept of charge-compensation in the synthesis of InSZ codoped with MoO_3, WO_3, $TaO_{2.5}$,

*e-mail address: honorato.piva@ua.pt

or $NbO_{2.5}$, intended to establish a route for the preparation of codoped InSZ-based TBCs. The selection of pentavalent oxides is based on its good performance in YSZ[9,10], in addition, it is explored further effects in the preparation of stabilized zirconia by charge-compensation using hexavalent ions. Moreover, we compared the effects of two different dehydration techniques applied to the coprecipitated gels to provide nanocrystalline powders with high specific surface area of these materials.

2. Material and methods

2.1 Synthesis by coprecipitation

The initial raw materials were: $ZrCl_4$ (99.5%), $InCl_3$ (99.99%), $NbCl_5$ (99.9%), $TaCl_5$ (99.99%), $(NH_4)_6Mo_7O_{24}\bullet 4H_2O$ (>99.9%), and $(NH_4)_6W_{12}O_{39}\bullet 4.7H_2O$ (>99.9%). The compositions studied in this paper are shown in Table 1. The molar concentrations of the dopants in InSZ were adjusted respecting the charge-compensating mechanism[10,21–23]. In this mechanism, we consider the partial substitution of Zr^{4+} host by In^{3+} acceptor ions along with the consequent compensation for Ta^{5+}/Nb^{5+} or W^{6+}/Mo^{6+} donor ions. For zirconia stabilized with $InO_{1.5}$ + $TaO_{2.5}/NbO_{2.5}$, the molar ratio of the cations was maintained at 1:1 (In^{3+}:Ta^{5+}/Nb^{5+}). This ratio can be understood through the Kröger-Vink notation[24] in Eqs. 1 and 2 wherein electroneutrality is achieved in case the doped acceptor and donor ions are in the same ratio. In the case of zirconia codoped with $InO_{1.5}$ + WO_3/MoO_3, the concentration of the doping ions was maintained at the ratio of 2:1 (In^{3+}:W^{6+}/Mo^{6+}). This ratio results from the fact that the incorporation of two In^{3+} ions in the zirconia network requires one W^{6+}/Mo^{6+} to reach electroneutrality without creating oxygen vacancies, as can be seen in Eqs. 3 and 4.

$$In_2O_3 + (Ta/Nb)_2O_5 \xrightarrow{ZrO_2} 2In'_{Zr} + 2(Ta/Nb)^{\bullet}_{Zr} + 8O^{x}_{O} \quad (1)$$

$$\left[In'_{Zr}\right] = \left[(Ta/Nb)^{\bullet}_{Zr}\right] \quad (2)$$

Table 1. Compositions of codoped InSZ samples and corresponding codes used in this work. The numbers in front of the chemical elements indicate their molar percentage. Due to the same molar ratio, only a single number is shown in the codes of the pentavalently doped compositions.

Composition*	Code
$(ZrO_2)_{0.940}(InO_{1.5})_{0.030}(TaO_{2.5})_{0.030}$	3InTaSZ
$(ZrO_2)_{0.880}(InO_{1.5})_{0.060}(TaO_{2.5})_{0.060}$	6InTaSZ
$(ZrO_2)_{0.820}(InO_{1.5})_{0.090}(TaO_{2.5})_{0.090}$	9InTaSZ
$(ZrO_2)_{0.940}(InO_{1.5})_{0.030}(NbO_{2.5})_{0.030}$	3InNbSZ
$(ZrO_2)_{0.880}(InO_{1.5})_{0.060}(NbO_{2.5})_{0.060}$	6InNbSZ
$(ZrO_2)_{0.820}(InO_{1.5})_{0.090}(NbO_{2.5})_{0.090}$	9InNbSZ
$(ZrO_2)_{0.910}(InO_{1.5})_{0.060}(MoO_3)_{0.030}$	6In3MoSZ
$(ZrO_2)_{0.865}(InO_{1.5})_{0.090}(MoO_3)_{0.045}$	9In4.5MoSZ
$(ZrO_2)_{0.910}(InO_{1.5})_{0.060}(WO_3)_{0.030}$	6In3WSZ
$(ZrO_2)_{0.865}(InO_{1.5})_{0.090}(WO_3)_{0.045}$	9In4.5WSZ

* $(ZrO_2)_{0.940}(InO_{1.5})_{0.030}(TaO_{2.5})_{0.030}$ is: 94 mol% ZrO_2 + 3 mol% $InO_{1.5}$ + 3 mol% $TaO_{2.5}$

$$In_2O_3 + (W/Mo)O_3 \xrightarrow{ZrO_2} 2In'_{Zr} + (W/Mo)^{\bullet\bullet}_{Zr} + 6O^{x}_{O} \quad (3)$$

$$\left[In'_{Zr}\right] = 2\left[(W/Mo)^{\bullet\bullet}_{Zr}\right] \quad (4)$$

Codoped InSZ gels were synthesized by coprecipitation. For the synthesis of InTaSZ and InNbSZ-derived compositions, all precursors were mixed together in distilled and deionized water and stirred for 10 min at 25 ºC to obtain a 0.1M solution. The prepared precursor solution was added dropwise at rates of 2–8 mLmin^{-1} into a vigorously stirred solution of aqueous ammonia (28–30% NH_3) with pH value of 11.8, in which the coprecipitation took place. The gel was then left without stirring to settle for 48 h in the precipitating solution at room temperature. Following this process, the precipitate was filtered and washed eight times with water. In the first two water-washing steps, a solution of 1M NH_4OH was used to prevent loss of cations. The following six washes were performed with distilled water until the absence of Cl^- ions was detected (monitored by means of 1M $AgNO_3$ solution).

In the case of InMoSZ and InWSZ-derived compositions, since precipitation of MoO_3 and WO_3 does not occur in basic medium, their precipitation was performed separately in acid medium and then the precipitate was added in the appropriate amount to the water-washed InSZ gel. For the precipitation of MoO_3[25], initially, 0.2M $(NH_4)_6Mo_7O_{24}\bullet 4H_2O$ solution in distilled water was stirred for 20 min at 25 °C. Once homogenized, HNO_3 (64–66%) was used as precipitating agent and added in a dropwise manner to the ammonium-molybdate solution. This solution was magnetically stirred for 30 min at 80 °C, corresponding to the appropriate conditions at which precipitation of MoO_3 could be observed. The amount of HNO_3 was defined by using Reaction 5. For the precipitation of WO_3[26], identical conditions were applied as in case of MoO_3. The precursor was $(NH_4)_6W_{12}O_{39}\bullet 4.7H_2O$ and HCl (36.5–38%) was used as precipitating agent. The amount of HCl was defined according to Reaction 6, although excess of HCl was needed until yellow precipitates of WO_3 started to appear.

$$(NH_4)_6Mo_7O_{24}\bullet 4H_2O_{(aq)} + 6\,HNO_{3\,(aq)} \rightarrow 7\,MoO_3\bullet xH_2O_{(s)} + 6\,NH_4NO_{3\,(aq)} + 7\,H_2O_{(aq)} \quad (5)$$

$$(NH_4)_6W_{12}O_{39}\bullet 4.7H_2O_{(aq)} + 6\,HCl_{(aq)} \rightarrow 12\,WO_3\bullet xH_2O_{(s)} + 6\,NH_4Cl_{(aq)} + 7.7\,H_2O_{(aq)} \quad (6)$$

Once the codoped InSZ gels were synthesized, the effects of the dehydration techniques ethanol washing followed by azeotropic distillation (EW/AD) and freeze drying (FD) were compared. For EW/AD, the gels were first washed twice with ethanol for 30 min under stirring, then left to settle for 1 h, and filtered. The mass ratio of 1:2.5 (gel/ethanol) was used[27]. In the next step, the gels were mixed with *iso*-butanol in the mass ratio of 1:1 (gel/butanol), vigorously stirred for 1 h and submitted to azeotropic distillation. For FD dehydration, a Liotop freeze-dryer model L101 was used. Initially, the gels were cooled in liquid nitrogen (–196 ºC) for 5 min. The condenser temperature and storage camera were kept at –52 and 20 °C, respectively. Vacuum of 5 Pa was applied to the storage camera, and the entire freeze-drying process took 48 h. Finally, both EW/AD and FD-derived powders were calcined at 600 °C for 1 h with heating/cooling rates of 3 °C min^{-1}.

2.2. Powder characterization

The crystal structures of the samples were identified by X-ray diffraction (XRD) using a diffractometer model Siemens D5005 in Bragg-Brentano geometry with CuKα radiation in the 2θ range from 5 to 85º and at the scan rate of 2º min^{-1}. The fraction of tetragonal zirconia ($v_t = 1 - v_m$) existent in the calcined powders was determined following the Eqs. 7 and 8 described by Toraya et al.[28], where X_m is the integration of the intensities ratio and I represent the diffraction intensity of the respective lattice plane for I_m(monoclinic) and I_t(tetragonal) phases. For the samples composed of the t- phase, the crystallite size was measured by the Scherrer equation[29] in the $(101)_t$ reflection of the tetragonal phase. Raman spectra of the calcined samples were obtained with a Renishaw inVia micro-spectrometer at 25 °C. Excitation was performed using the 532 nm line and spectra were recorded in the spectral range between 1 and 1000 cm^{-1}.

$$v_m = \frac{1.311X_m}{1+0.311X_m} \quad (7)$$

$$X_m = \frac{I_m(\bar{1}11)+I_m(111)}{I_m(\bar{1}11)+I_m(111)+I_t(101)} \quad (8)$$

Fourier-transform infrared (FT-IR) spectra were recorded with a Thermo Scientific Nicolet™ 6700 spectrometer with 2 cm^{-1} resolution and 128 scans in the spectral range between 400 and 4000 cm^{-1}. Powder samples were mixed with KBr in a mass weight of 1:1 for FT-IR recording. Differential scanning calorimetry and thermogravimetric analysis (DSC/TG) of the gels were recorded with the heating rate of 10 °C min^{-1} up to 700 °C in an Ar atmosphere.

The specific surface areas S_{BET} of the calcined powders were measured by the Brunauer-Emmett-Teller (BET) method using N_2 adsorption-desorption (Micrometrics Gemini 2370 V1.02). The particle size and morphology of the samples were observed by transmission electron microscopy (TEM) with the instrument FEI Tecnai G^2 F20 at the acceleration voltage of 200 kV. For TEM observations, the powders were ultrasonically dispersed in acetone for 10 min and then dripped onto carbon films on top of copper grids (200 mesh) and dried at room temperature.

3. Results and Discussion

3.1. Crystallization and phase formation

As shown in Fig. 1, the uncalcined gels dehydrated by EW/AD and FD are amorphous, regardless of the concentration of the stabilizer alloyed. For compositions containing 3 mol% of $InO_{1.5}$, it is possible to observe some

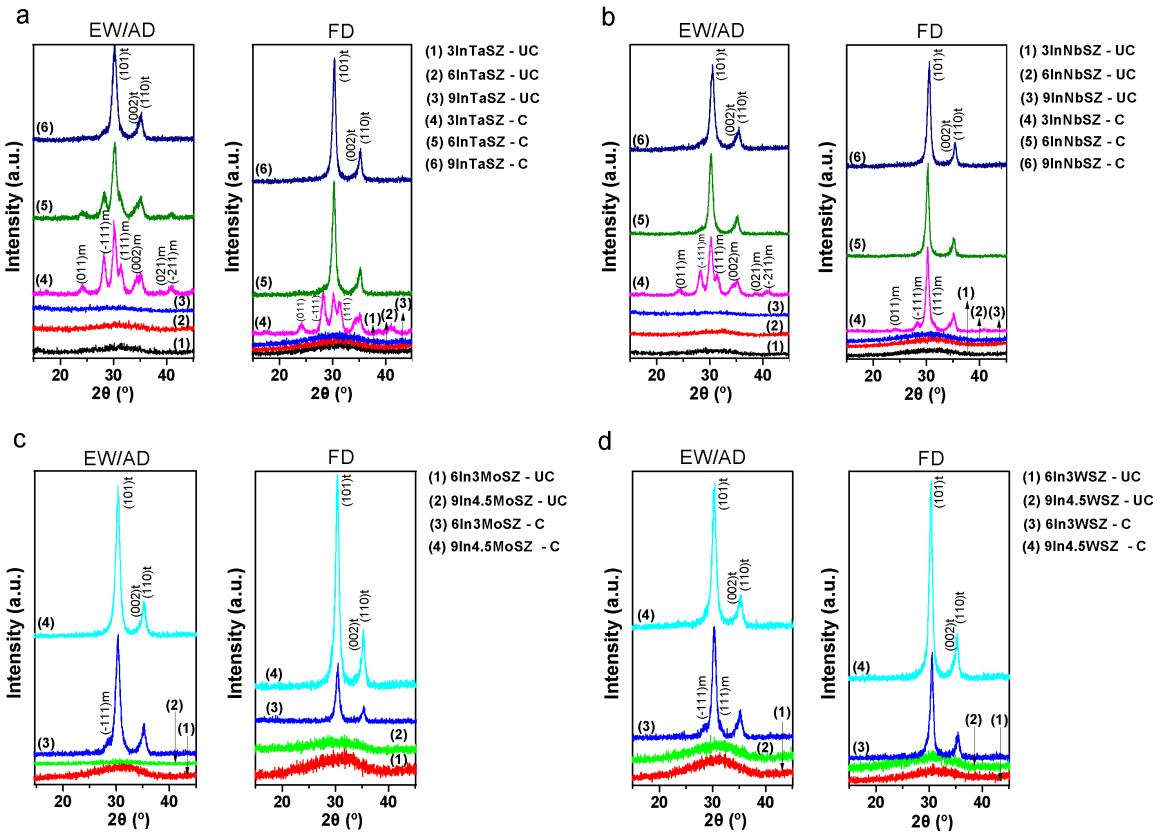

Fig. 1 XRD patterns after EW/AD and FD dehydration for the systems: (a) InTaSZ, (b) InNbSZ, (c) InMoSZ, and (d) InWSZ. The subscripts t and m represent the tetragonal and monoclinic phases, respectively. Each composition is represented by numbers and labeled by either UC - uncalcined or C - calcined at 600 ºC for 1 h.

retention of the tetragonal symmetry (PDF No. 79-1771) after calcination at 600 ºC. However, in these compositions, the concentration of the stabilizer is insufficient for the total stabilization of the t- phase and, therefore, the monoclinic phase (PDF No. 37-1484) of zirconia (m-) was detected (Fig. 1a and b). For the FD-dehydrated samples, increasing the concentration of $InO_{1.5}$ to 6 mol% generates exclusively the t- phase without small background peaks $(-111)_m$ and $(111)_m$ of the monoclinic phase. With respect to the samples dehydrated by EW/AD, the complete stabilization of the t- phase was only achieved for samples with 9 mol% of $InO_{1.5}$ plus additional charge-compensating dopants: 9 mol% of $NbO_{2.5}/TaO_{2.5}$ or 4.5 mol% of MoO_3/WO_3. DSC analysis for the InNbSZ compositions (Fig. 2) shows that the crystallization temperature rises with increasing $InO_{1.5}$ and $NbO_{2.5}$ concentration. The crystallization at 491 °C for the 9 mol% InNbSZ sample is higher than 480 °C[30] and 486 ºC[27] recently reported for the crystallization of tetragonal YSZ. Comparing these DSC results with the XRD patterns shown in Fig. 1b, it can be seen that increased crystallization temperatures correspond to the stabilization of the t- phase, in agreement with the results obtained for the Y_2O_3–ZrO_2 system, as reported by Haberko et al.[31].

From the XRD patterns in Fig. 1, the distinction between tetragonal and cubic phase (c-) is not apparent, since the distinction between the peaks $(002)_t/(110)_t$ at $2\theta \approx 35°$ cannot be observed unambiguously because of peak-broadening effects[32,33]. For this reason, visible Raman spectra were used to observe the existence of the single t- phase[2,34]. Raman spectra for InTaSZ compositions are shown in Fig. 3. It can be seen in Fig. 3a that the 3InTaSZ sample gives major bands at 176, 188, 219, 330, 343, 381, 460, 501, 538, 558, and 618 cm^{-1}, which are characteristic bands of the m- phase. These are 11 of the 16 Raman modes predicted by group theory for monoclinic zirconia[2,35–37]. The detection of the m- phase in the Raman spectra of the 3InTaSZ sample is in agreement with the presence of 58 vol% of monoclinic zirconia calculated on the basis of XRD. In the case of the 9InTaSZ sample (Fig. 3c), bands at 147, 276, 310, 470, and 637 cm^{-1} represent 5 of the 6 Raman-active modes predicted by group theory for tetragonal symmetry[36,38,39]. Similar Raman spectra for YSZ were recorded by Ghosh et al.[33]. Therefore, the 9InTaSZ sample is composed exclusively by the t- phase and we can consider that this holds true also for the others EW/AD dehydrated samples: 9InNbSZ, 9In4.5MoSZ, and 9In4.5WSZ due the similarity of their XRD patterns (Fig. 1) and the same $InO_{1.5}$ concentration. Moreover, the Raman spectrum of the 9InTaSZ sample does not provide evidence for the existence of the c- phase[32,35,36,39], since cubic symmetry must theoretically be reflected by a single broad band between 400 and 670 cm^{-1}, which is not observed in Fig. 3c.

A comparison of the XRD and Raman results reveals that alloying 9 mol% of $InO_{1.5}$ into zirconia and dehydrated by EW/AD provides the complete stabilization of the t- phase. On the other hand, the charge-compensating dopants on definition of crystal structure could not be observed in the present work due the lower calcination temperature. This condition does not allow the codopants diffusion, especially for molybdenum and tungsten oxides, that were not coprecipitated with indium oxide. Li et al.[21] found that the substitution of Zr^{4+} host ions by Nb^{5+} (and also Ta^{5+}) in YSZ increases the temperature of the t→m transformation. However, these changes only occur after thermal treatments at 1500 ºC, a condition at which Nb^{5+}/Ta^{5+} ions are in substitutional positions with respect to the cation network[22,40,41]. We observed through TEM images (not shown) the existence of isolated Nb_2O_5 and Ta_2O_5 particles in the calcined 9InTaSZ and 9InNbSZ samples. The presence of these particles represents an evidence that at low calcination temperatures, the Nb^{5+}/Ta^{5+} ions are not completely alloyed into the InSZ network. In the case of hexavalent oxides, the effect of MoO_3 and WO_3 in the retention of the t- phase has been reported by Reddy and Reddy[42]. Comparing MoO_3/ZrO_2 and WO_3/ZrO_2 catalysts, the authors observed that MoO_3 seems to be more effective in the retention of the tetragonal symmetry of zirconia. However, no apparent difference between MoO_3 and WO_3 regarding

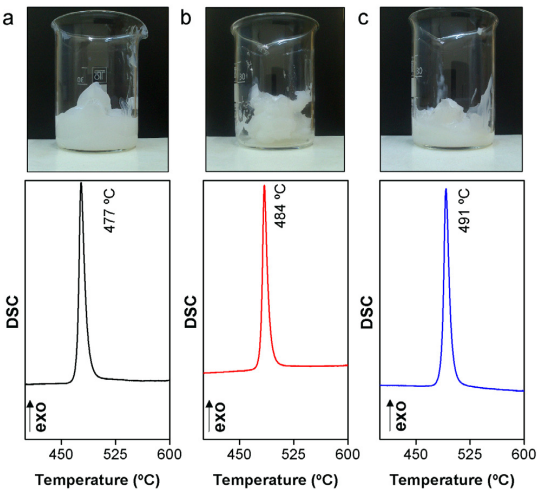

Fig. 2 Crystallization temperature for: (a) 3InNbSZ, (b) 6InNbSZ, and (c) 9InNbSZ. These DSC analyses were performed on as-precipitated gels dried at 100 ºC for 24 h.

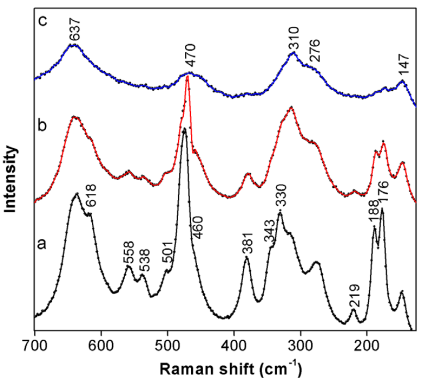

Fig. 3 Raman spectra of EW/AD dehydrated samples after calcination at 600 ºC for 1 h: (a) 3InTaSZ, (b) 6InTaSZ, and (c) 9InTaSZ.

the stabilization of the t- phase in InSZ was observed here (see Fig. 1c and d). Therefore, as in the case of pentavalent oxides, the effects of the charge-compensating dopants appear to be secondary in relation to the $InO_{1.5}$ concentration at low calcination temperature.

3.2. Powder characteristics after dehydration

The powder characteristics after EW/AD and FD dehydration are shown in Table 2. The specific surface-area values of the samples dehydrated by EW/AD were considerably higher than those obtained after FD in agreement with a previous work[43]. Practically the same S_{BET} values were achieved for 9InTaSZ and 9InNbSZ, whereas the Nb_2O_5 and Ta_2O_5 oxides can be considered as having similar effects in the gel formation during coprecipitation. On the other hand, InSZ codoped with MoO_3 and WO_3 presented higher S_{BET} values than those observed for pentavalent oxides. The highest S_{BET} of 106.1 $m^2\ g^{-1}$ was found in the 9In4.5MoSZ sample after EW/AD dehydration. The fact that the addition of hexavalent oxides increases S_{BET} was also observed in zirconia-supported catalysts by Scheithauer et al.[44]. The authors suggested that the formation of WO_x clusters anchored on the zirconia surface provides W–O–W and W=O bonds responsible for the lowering of the diffusion, thus inhibiting coalescence of zirconia crystallites and maintaining high specific surface area. Similar S_{BET} values found for the 9In4.5WSZ and 9In4.5MoSZ samples show an equivalent behavior when WO_3 or MoO_3 are alloyed into InSZ.

Fig. 4 shows TEM images of the calcined 9InTaSZ sample after different dehydration techniques have been applied. The images obtained after EW/AD (Fig. 4a) indicate a low level of agglomeration. This fact is consistent with the high S_{BET} values presented in Table 2. In contrast, the 9InTaSZ sample dehydrated by FD exhibited a higher level of agglomeration, as shown in Fig. 4b, whereas the lower S_{BET} values after FD is a direct effect of the formation of hard agglomerates. For both EW/AD and FD powders, the electron diffraction patterns show tetragonal zirconia[45,46], along with the interplanar spacing of 0.29 nm for the (101)$_t$ plane, once again consistent with the values reported for tetragonal symmetry[47,48].

For all the samples, the crystallite size was smaller after EW/AD dehydration (see Table 2). In the 9InTaSZ powders dehydrated by EW/AD, the small crystallite size of 8.4 nm calculated by the Scherrer formula is in agreement with the TEM observation (Fig. 4a). Furthermore, the high degree of agglomeration after FD dehydration is probably the main cause for complete stabilization of the t- phase at concentrations of $InO_{1.5}$ that are lower than those required after EW/AD. Apparently, it is a result of the constriction exerted on the dense agglomerates of zirconia crystallites in case of FD. More details of this stabilization mechanism can be found in the work of Shukla et al.[49].

Table 2. Characteristics of InSZ codoped samples dehydrated by EW/DA and FD after calcination.

Code and dehydration technique		Content of t- phase (vol%)	S_{BET} ($m^2.g^{-1}$)	Crystallite size (nm)
3InTaSZ	FD	29	-	-
	EW/AD	42	-	-
6InTaSZ	FD	100	-	-
	EW/AD	51	-	-
9InTaSZ	FD	100	64.2	11.9
	EW/AD	100	84.6	8.4
3InNbSZ	FD	74	-	-
	EW/AD	48	-	-
6InNbSZ	FD	100	-	-
	EW/AD	100	-	-
9InNbSZ	FD	100	60.5	12.0
	EW/AD	100	85.9	9.0
6In3MoSZ	FD	100	-	-
	EW/AD	75	-	-
9In4.5MoSZ	FD	100	87.4	10.2
	EW/AD	100	106.1	8.7
6In3WSZ	FD	100	-	-
	EW/AD	72	-	-
9In4.5WSZ	FD	100	85.3	12.5
	EW/AD	100	103.5	9.1

3.3. Modifications in the gels after EW/AD and FD

The DSC/TG curve of the 6InNbSZ sample dehydrated by FD (Fig. 5a) shows two peaks. First, an endothermic peak at ~130 °C originating from the elimination of physically adsorbed water[50–52]. Water removal progresses continuously up to 495 °C and, at this temperature, an exothermic peak due the crystallization of zirconia can be observed. For this FD dehydrated sample, the mass loss of 17.2 wt% between 25 and 495 °C occurs because of desorption of water and removal of hydroxyl groups (OH^-)[30]. In contrast to FD, the dehydration of the 6InNbSZ sample by EW/AD leads to significant changes in the DSC/TG curve (Fig. 5b). The broad endothermic peak at ~130 °C after FD dehydration is replaced by a narrow peak at 100 °C, which is characteristic of alcohol dehydration[53]. Ethanol washing prior to azeotropic distillation led to chemical changes in the gel, as reflected by the endothermic peak at 290 °C. This endothermic reaction is due to the replacement of original hydroxyl by ethoxy groups ($CH_3CH_2O^-$) during prior washing of the gels with ethanol[27]. Further effects of the azeotropic distillation with butanol can be observed in the DSC/TG curve in form of one endothermic peaks at 250 °C and another less visible one around 300 °C, all related to the removal of butoxy groups ($C_4H_9O^-$)[54]. Thus, the interaction between codoped hydroxide and organic solvents incorporated by EW/AD seems to be responsible for the high specific surface area, low crystallite size, and low agglomeration level, as presented in Table 2.

These chemical interactions between gel and solvent can also be observed in the FT-IR spectra. As shown in Fig. 6a, the FT-IR spectrum of the 6InNbSZ sample dehydrated by FD presents a band at 3400 cm^{-1} due to the stretching vibration of structural –OH groups and adsorbed water molecules[55]. The band at 1630 cm^{-1} accounts for the vibration of Zr–OH in the codoped InSZ hydroxide[51,56]. Furthermore, we can observe a band at 1360 cm^{-1} which indicates the presence of carbonate species resulting from the incorporation of atmospheric CO_2 into the gels[48]. With respect to the gel after EW/AD dehydration

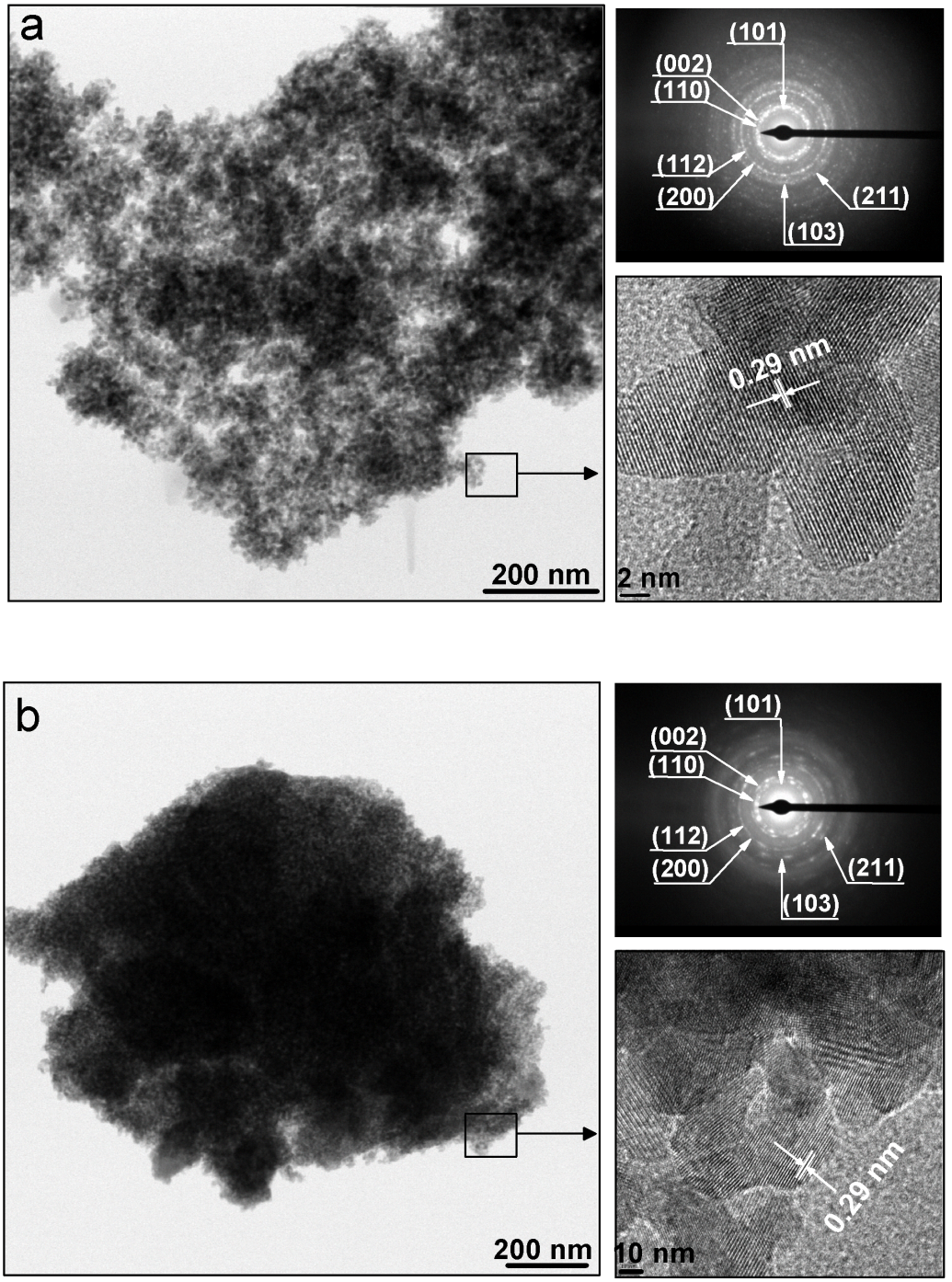

Fig. 4 TEM images of 9InTaSZ dehydrated by (a) EW/AD and (b) FD. Electron diffraction patterns and high-resolution images are shown for the two dehydration techniques.

(Fig. 6b), a band at 2971 cm^{-1} characteristic of C–H groups after ethanol washing, and a small band at 1159 cm^{-1} probably originating from adsorbed ethanol[55] are present. Azeotropic distillation with butanol provided an additional small band at 2861 cm^{-1}, corresponding also to C–H groups, although the characteristic band at 1446 cm^{-1} reflecting C–C units from adsorbed butanol cannot be identified because of the overlap with the zirconium-hydroxide region[57]. These bands provide further evidence regarding the adsorption of ethoxy and butoxy organic complexes after EW/AD dehydration, in accordance with the DSC/TG curves (Fig. 5). Indeed, the better powder characteristics provided by this technique is a result of the chemical modification of the InSZ codoped gels.

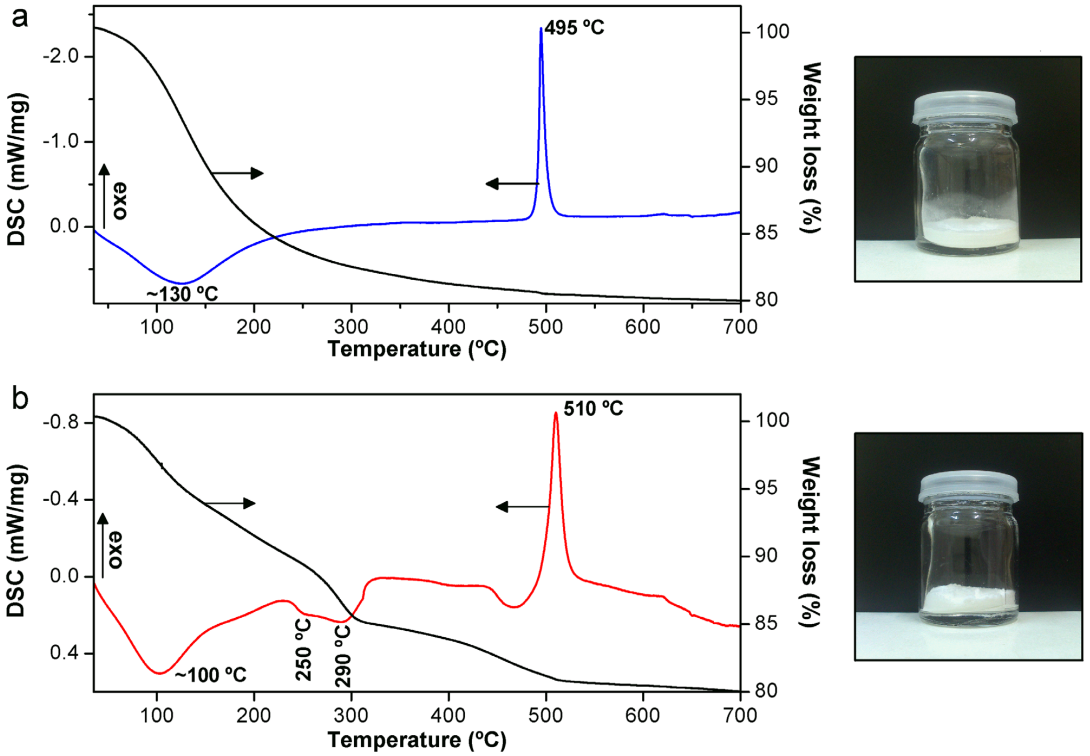

Fig. 5 DSC/TG curves of the 6InNbSZ sample after the application of different dehydration techniques: (a) FD and (b) EW/AD.

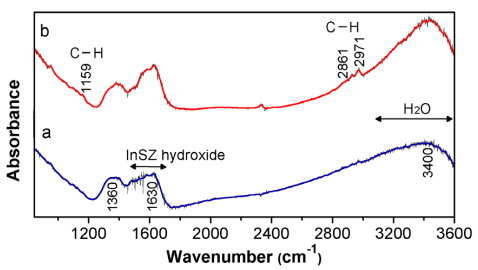

Fig. 6 FT-IR spectra of the 6InNbSZ sample dehydrated by (a) FD and (b) EW/AD.

4. Conclusions

A route for producing tetragonal india-stabilized zirconia by coprecipitation and codoping with hexavalent (WO_3, MoO_3) or pentavalent ($NbO_{2.5}$, $TaO_{2.5}$) oxides was presented. The effect of charge-compensating oxides in stabilizing the tetragonal zirconia phase seems to be secondary in relation to the amount of $InO_{1.5}$, which probably occurs due to the low calcination temperature used, thus not allowing direct observation of the effect of codopants. However, WO_3 and MoO_3 oxides are more effective in promoting modifications in the gels, leading to specific surface areas of up to 106.1 $m^2.g^{-1}$. Ethanol washing followed by azeotropic distillation is the preferable dehydration technique, rather than freeze-drying, to produce highly non-agglomerated powders of these systems. The effectiveness of this technique is derived by the substitution of surface –OH group in the InSZ codoped hydroxide for CH_3CH_2O– after ethanol washing and further C_4H_9O– after azeotropic distillation. It is important to note that further exploration regarding the high-temperature stability, long time phase stability, ability to be deposited as a homogeneous coating, and others properties, are required to evaluate the adequacy of 9In4.5MoSZ, 9In4.5WSZ, 9InTaSZ, and 9InNbSZ as TBC materials.

Acknowledgments

The authors acknowledge the FAPESP (No. 2013/14189-8) for the financial support provided for this research.

References

1. Raghavan S and Mayo MJ. The hot corrosion resistance of 20 mol% $YTaO_4$ stabilized tetragonal zirconia and 14 mol% Ta_2O_5 stabilized orthorhombic zirconia for thermal barrier coating applications. *Surface and Coatings Technology*. 2002; 160(2):187-196. http://dx.doi.org/10.1016/S0257-8972(02)00393-6.
2. Mayoral MC, Andrés JM, Bona MT, Higuera V and Belzunce FJ. Yttria stabilized zirconia corrosion destabilization followed by Raman mapping. *Surface and Coatings Technology*. 2008; 202(21):5210-5216. http://dx.doi.org/10.1016/j.surfcoat.2008.06.050.
3. Mutasim Z and Brentnall W. Thermal barrier coatings for industrial gas turbine applications: An industrial note. *Journal of Thermal Spray Technology.* 1997; 6(1):105-108.

4. Nagelberg AS. Destabilization of Yttria-Stabilized Zirconia Induced by Molten Sodium Vanadate-Sodium Sulfate Melts. *Journal of the Electrochemical Society*. 1985; 132:2502-2507.
5. Huang X, Zakurdaev A and Wang D. Microstructure and phase transformation of zirconia-based ternary oxides for thermal barrier coating applications. *Journal of Materials Science*. 2008; 43(8):2631-2641. http://dx.doi.org/10.1007/s10853-008-2480-x.
6. Zhou Y, Xiang H and Feng Z. Theoretical investigation on mechanical and thermal properties of a promising thermal barrier material: $Yb_3Al_5O_{12}$. *Journal of Materials Science and Technology*. 2014; 30(7):631-638. http://dx.doi.org/10.1016/j.jmst.2014.06.007.
7. Li D and Li M. Porous Y_2SiO_5 Ceramic with low thermal conductivity. *Journal of Materials Science and Technology*. 2012; 28(9):799-802. http://dx.doi.org/10.1016/S1005-0302(12)60133-9.
8. Levi CG. Emerging materials and processes for thermal barrier systems. *Current Opinion in Solid State and Materials Science*. 2004; 8(1):77-91. http://dx.doi.org/10.1016/j.cossms.2004.03.009.
9. Pitek FM and Levi CG. Opportunities for TBCs in the ZrO_2–$YO_{1.5}$–$TaO_{2.5}$ system. *Surface and Coatings Technology*. 2007; 201(12):6044-6050. http://dx.doi.org/10.1016/j.surfcoat.2006.11.011.
10. Raghavan S, Wang H, Dinwiddie RB, Porter WD, Vassen R, Stöver D, et al. Ta_2O_5/Nb $_2O_5$ and Y_2O_3 Co-doped zirconias for thermal barrier coatings. *Journal of the American Ceramic Society*. 2004; 87(3):431-437.
11. Zhong XH, Wang YM, Xu ZH, Zhang YF, Zhang JF and Cao XQ. Hot-corrosion behaviors of overlay-clad yttria-stabilized zirconia coatings in contact with vanadate–sulfate salts. *Journal of the European Ceramic Society*. 2010; 30(6):1401-1408. http://dx.doi.org/10.1016/j.jeurceramsoc.2009.10.017.
12. Mohan P, Yuan B, Patterson T, Desai VH and Sohn YH. Degradation of yttria-stabilized zirconia thermal barrier coatings by vanadium pentoxide, phosphorous pentoxide, and sodium sulfate. *Journal of the American Ceramic Society*. 2007; 90(11):3601-3607. http://dx.doi.org/10.1111/j.1551-2916.2007.01941.x.
13. Li S, Liu ZG and Ouyang JH. Hot corrosion of $(Sm_{1-x}Yb_x)_2Zr_2O_7$ (x=0, 0.5, 1.0) ceramics against V_2O_5 molten salt in air at 800°C. *International Journal of Applied Ceramic Technology.* 2012; 9:149-158. http://dx.doi.org/10.1111/j.1744-7402.2011.02623.x.
14. Jones RL and Williams CE. Hot corrosion studies of zirconia ceramics. *Surface and Coatings Technology*. 1987; 32(1):349-358. http://dx.doi.org/10.1016/0257-8972(87)90119-8.
15. Jones RL. Some aspects of the hot corrosion of thermal barrier coatings. *Journal of Thermal Spray Technology.* 1997; 6(1):77-84.
16. Jones RL and Mess D. India as a hot corrosion-resistant stabilizer for zirconia. *Journal of the American Ceramic Society*. 1992; 75:1818-1821. http://dx.doi.org/10.1111/j.1151-2916.1992.tb07202.x.
17. Jones RL, Reidy RF and Mess D. Vanadate Hot Corrosion behavior of India, Yttria-stabilized zirconia. *Journal of the American Ceramic Society*. 1993; 76:2660-2662. http://dx.doi.org/10.1111/j.1151-2916.1993.tb03995.x.
18. Sasaki K, Bohac P and Gauckler LJ. Phase Equilibria in the System ZrO_2-$InO_{1.5}$. *Journal of the American Ceramic Society*. 1993; 76:689-698.
19. Burns RP, DeMaria G, Drowart J and Inghram MG. Mass Spectrometric Investigation of the Vaporization of In_2O_3. *The Journal of Chemical Physics*. 1963; 38:1035-1036.
20. Hill MD, Phelps DP and Wolfe DE, editors. *Corrosion resistant thermal barrier coating materials for industrial gas turbine applications*. Hoboken, NJ: John WIley & Sons; 2009. v. 29, n. 4. (Advanced Ceramic Coatings and Interfaces III: Ceramic Engineeing and Science). http://dx.doi.org/10.1002/9780470456323.ch10.
21. Li P, Chen I-W and Penner-Hahn JE. Effect of dopants on zirconia stabilization-an x-ray absorption study: iii, charge-compensating dopants. *Journal of the American Ceramic Society*. 1994; 77:1289-1295. http://dx.doi.org/10.1111/j.1151-2916.1994.tb05404.x.
22. Kim D-J. Effect of Ta_2O_5, Nb_2O_5, and HfO_2 alloying on the transformability of Y_2O_3-stabilized tetragonal ZrO_2. *Journal of the American Ceramic Society*. 1990; 73:115-120.
23. Niu X, Xie M, Zhou F, Mu R, Song X and An S. Substituent influence of Yttria by Gadolinia on the tetragonal phase stability for Y_2O_3–Ta_2O_5–ZrO_2 ceramics at 1300 °C. *Journal of Materials Science and Technology*. 2014; 30(4):381-386. http://dx.doi.org/10.1016/j.jmst.2013.12.008.
24. Kröger FA and Vink HJ. Relations between the Concentrations of Imperfections in Crystalline Solids. *Solid State Physics*. 1956; 3:307-435.
25. Jittiarporn P, Sikong L, Kooptarnond K and Taweepreda W. Effects of precipitation temperature on the photochromic properties of h-MoO_3. *Ceramics International*. 2014; 40(8):13487-13495. http://dx.doi.org/10.1016/j.ceramint.2014.05.076.
26. Supothina S, Seeharaj P, Yoriya S and Sriyudthsak M. Synthesis of tungsten oxide nanoparticles by acid precipitation method. *Ceramics International*. 2007; 33(6):931-936. http://dx.doi.org/10.1016/j.ceramint.2006.02.007.
27. Patil SB, Jena AK and Bhargava P. Influence of ethanol amount during washing on deagglomeration of co-precipitated calcined nanocrystalline 3YSZ powders. *International Journal of Applied Ceramic Technology*. 2013; 10:E247-E257. http://dx.doi.org/10.1111/j.1744-7402.2012.02813.x.
28. Toraya H, Yoshimura M and Somiya S. Calibration curve for quantitative analysis of the monoclinic-tetragonal ZrO2 system by X-ray diffraction. *Journal of the American Ceramic Society.* 1984; 67(6):C–119-C–121. http://dx.doi.org/10.1111/j.1151-2916.1984.tb19715.x.
29. Scherrer P. Bestimmung der Grösse und der Inneren Struktur von Kolloidteilchen Mittels Röntgenstrahlen, Nachrichten von der Gesellschaft der Wissenschaften zu Göttingen. *Mathematisch-Physikalische Klasse.* 1918; 2:98-100.
30. Hsu Y-W, Yang K-H, Chang K-M, Yeh S-W and Wang M-C. Synthesis and crystallization behavior of 3mol% yttria stabilized tetragonal zirconia polycrystals (3Y-TZP) nanosized powders prepared using a simple co-precipitation process. *Journal of Alloys and Compounds*. 2011; 509(24):6864-6870. http://dx.doi.org/10.1016/j.jallcom.2011.03.162.
31. Haberko K, Ciesla A and Pron A. Sintering behaviour of yttria-stabilized zirconia powders prepared from gels. *Ceramics International*. 1975; 1(4):111-116.
32. Kontoyannis CG and Orkoula M. Quantitative determination of the cubic, tetragonal and monoclinic phases in partially stabilized zirconias by Raman spectroscopy. *Journal of Materials Science*. 1994; 29(20):5316-5320. http://dx.doi.org/10.1007/BF01171541.
33. Ghosh A, Suri AK, Pandey M, Thomas S, Rama Mohan TR and Rao BT. Nanocrystalline zirconia-yttria system–a Raman study. *Materials Letters*. 2006; 60(9-10):1170-1173. http://dx.doi.org/10.1016/j.matlet.2005.10.102.
34. Li C, Li M and Li CUV. Raman spectroscopic study on the phase transformation of ZrO_2, Y_2O_3-ZrO_2 and SO_4^{2-}/ZrO_2. *Journal of Raman Spectroscopy : JRS*. 2002; 33(5):301-308. http://dx.doi.org/10.1002/jrs.863.

35. Kontoyannis CG and Carountzos G. Quantitative determination of the cubic-to-monoclinic phase transformation in fully stabilized zirconias by Raman spectroscopy. *Journal of the American Ceramic Society*. 1994; 77:2191-2194. http://dx.doi.org/10.1111/j.1151-2916.1994.tb07117.x.

36. Perry CH, Liu D-W and Ingel RP. Phase Characterization of Partially Stabilized Zirconia by Raman Spectroscopy. *Journal of the American Ceramic Society*. 1985; 68:C–184-C–187.

37. Štefanić G, Musić S, Popović S and Sekulić A. FT-IR and laser Raman spectroscopic investigation of the formation and stability of low temperature t-ZrO_2. *Journal of Molecular Structure*. 1997; 408:391-394.

38. Anastassakis E, Papanicolaou B and Asher IM. Lattice dynamics and light scattering in Hafnia and Zirconia. *Journal of Physics and Chemistry of Solids*. 1975; 36:667-676.

39. Feinberg A and Perry CH. Structural disorder and phase transitions in ZrO_2-Y_2O_3 system. *Journal of Physics and Chemistry of Solids*. 1981; 42:513-518.

40. Kim D. Phase transformations of Y_2O_3 and Nb_2O_5 doped tetragonal zirconia during low temperature aging in air. *Solid State Ionics*. 1995; 80:67-73.

41. Kim D, Becher PF and Hubbard CR. Effect of Nb_2O_5 Alloying on Thermal Expansion Anisotropy of 2 mol% Y_2O_3-Stabilized Tetragonal ZrO_2. *Journal of the American Ceramic Society*. 1993; 76:2904-2908.

42. Reddy BM and Reddy VR. Influence of SO_4^{2-}, Cr_2O_3, MoO_3, and WO_3 on the stability of ZrO_2-tetragonal phase. *Journal of Materials Science Letters*. 2000; 19(9):763-765.

43. Piva RH, Piva DH, Pierri JJ, Montedo OR and Morelli MR. Azeotropic distillation, ethanol washing, and freeze drying on coprecipitated gels for production of high surface area 3Y–TZP and 8YSZ powders: A comparative study. *Ceramics International*. 2015; 41(10):14148-14156. http://dx.doi.org/10.1016/j.ceramint.2015.07.037.

44. Scheithauer M, Grasselli RK and Knözinger H. Genesis and structure of WO_x/ZrO_2 solid acid catalysts. *Langmuir*. 1998; 14(11):3019-3029.

45. Readey MJ, Lee R, Halloran JW and Heuer AH. Processing and sintering of ultrafine MgO-ZrO_2 and (MgO, Y_2O_3)-ZrO_2 powders. *Journal of the American Ceramic Society*. 1990; 73(6):1499-1503. http://dx.doi.org/10.1111/j.1151-2916.1990.tb09786.x.

46. Zaporina NA, Doynikova OA, Krumina AP, Bocharov DA and Grabis JP. Methods of electron microdiffraction and X-ray analysis in structure study of nanodisperse partially stabilized ZrO_2 powders. *Journal of Surface Investigation. X-ray, Synchrotron and Neutron Techniques*. 2009; 3(3):464-467. http://dx.doi.org/10.1134/S1027451009030227.

47. Ryu J-H, Kil H-S, Song J-H, Lim D-Y and Cho S-B. Glycothermal synthesis of 3mol% yttria stabilized tetragonal ZrO_2 nano powders at low temperature without mineralizers. *Powder Technology*. 2012; 221:228-235. http://dx.doi.org/10.1016/j.powtec.2012.01.006.

48. Wang H, Li G, Xue Y and Li L. Hydrated surface structure and its impacts on the stabilization of t-ZrO_2. *Journal of Solid State Chemistry*. 2007; 180(10):2790-2797. http://dx.doi.org/10.1016/j.jssc.2007.08.015.

49. Shukla S, Seal S, Vij R, Bandyopadhyay S and Rahman Z. Effect of nanocrystallite morphology on the metastable tetragonal phase stabilization in zirconia. *Nano Letters*. 2002; 2(9):989-993. http://dx.doi.org/10.1021/nl025660b.

50. Jakubus P, Adamski A, Kurzawa M and Sojka Z. Texture of zirconia obtained by forced hydrolysis of $ZrOCl_2$ solutions Influence of aging on thermal behavior. *Journal of Thermal Analysis and Calorimetry*. 2003; 72(1):299-310.

51. Rezaei M, Alavi SM, Sahebdelfar S, Yan Z-F, Teunissen H, Jacobsen JH, et al. Synthesis of pure tetragonal zirconium oxide with high surface area. *Journal of Materials Science*. 2007; 42(4):1228-1237. http://dx.doi.org/10.1007/s10853-006-0079-7.

52. Tallón C, Moreno R and Nieto MI. Synthesis of ZrO_2 nanoparticles by freeze drying. *International Journal of Applied Ceramic Technology.* 2009; 6(2):324-334. http://dx.doi.org/10.1111/j.1744-7402.2008.02279.x.

53. Qiu H, Gao L, Feng C, Guo J and Yan D. Preparation and characterization of nanoscale Y-TZP powder by heterogeneous azeotropic distillation. *Journal of Materials Science*. 1995; 30(21):5508-5513.

54. Yao H-C, Wang X-W, Dong H, Pei R-R, Wang J-S and Li Z-J. Synthesis and characteristics of nanocrystalline YSZ powder by polyethylene glycol assisted coprecipitation combined with azeotropic-distillation process and its electrical conductivity. *Ceramics International*. 2011; 37(8):3153-3160. http://dx.doi.org/10.1016/j.ceramint.2011.05.055.

55. Kaliszewski MS and Heuer AH. Alcohol interaction with zirconia powders. *Journal of the American Ceramic Society*. 1990; 73:1504-1509.

56. Sarkar D, Mohapatra D, Ray S, Bhattacharyya S, Adak S and Mitra N. Synthesis and characterization of sol–gel derived ZrO_2 doped Al_2O_3 nanopowder. *Ceramics International*. 2007; 33(7):1275-1282. http://dx.doi.org/10.1016/j.ceramint.2006.05.002.

57. Shan H and Zhang Z. Preparation of nanometre-sized ZrO_2/Al_2O_3 powders by heterogeneous azeotropic distillation. *Journal of the European Ceramic Society*. 1997; 17(5):713-717. http://dx.doi.org/10.1016/S0955-2219(96)00087-8.